J|A|C|S
ARTICLES
Published on Web 05/25/2006

A Solid-State ^{95}Mo NMR and Computational Investigation of Dodecahedral and Square Antiprismatic Octacyanomolybdate(IV) Anions: Is the Point-Charge Approximation an Accurate Probe of Local Symmetry?

Michelle A. M. Forgeron and Roderick E. Wasylishen*

Contribution from the Department of Chemistry, Gunning/Lemieux Chemistry Centre, University of Alberta, Edmonton, Alberta, Canada T6G 2G2

Received January 6, 2006; Revised Manuscript Received April 6, 2006; E-mail: roderick.wasylishen@ualberta.ca

Abstract: Solid-state ^{95}Mo NMR spectroscopy is shown to be an efficient and effective tool for analyzing the diamagnetic octacyanomolybdate(IV) anions, $Mo(CN)_8^{4-}$, of approximate dodecahedral, D_{2d}, and square antiprismatic, D_{4d}, symmetry. The sensitivity of the Mo magnetic shielding (σ) and electric field gradient (EFG) tensors to small changes in the local structure of these anions allows the approximate D_{2d} and D_{4d} $Mo(CN)_8^{4-}$ anions to be readily distinguished. The use of high applied magnetic fields, 11.75, 17.63 and 21.1 T, amplifies the overall sensitivity of the NMR experiment and enables more accurate characterization of the Mo σ and EFG tensors. Although the magnitudes of the Mo σ and EFG interactions are comparable for the D_{2d} and D_{4d} $Mo(CN)_8^{4-}$ anions, the relative values and orientations of the principal components of the Mo σ and EFG tensors give rise to ^{95}Mo NMR line shapes that are significantly different at the fields utilized here. Quantum chemical calculations of the Mo σ and EFG tensors, using zeroth-order regular approximation density functional theory (ZORA DFT) and restricted Hartree−Fock (RHF) methods, have also been carried out and are in good agreement with experiment. The most significant and surprising result from the DFT and RHF calculations is a significant EFG at Mo for an isolated $Mo(CN)_8^{4-}$ anion possessing an ideal square antiprismatic structure; this is contrary to the point-charge approximation, PCA, which predicts a zero EFG at Mo for this structure.

1. Introduction

Interest in transition metal cyanides dates back to the early 1700s with the discovery of Prussian Blue.[1] In recent years, interest in cyanometalates has been revived, in part, due to the utility of these anions as the building blocks of magnetic clusters and networks.[2−6] The classic textbook[7] examples of eight-coordination transition metal cyanides are the molybdenum and tungsten octacyanide anions,[8,9] which have been known for nearly 100 years.[10] These anions exist in both diamagnetic and paramagnetic forms, where the metal is in a formal oxidation state of +4 or +5, respectively.[1,7,11] Of particular interest is the ability of the (Mo, W) octacyanide anions to adopt different molecular arrangements which may be approximately[13] described by the polyhedra illustrated in Figure 1. In the solid state, the diamagnetic Mo(IV) analogue, [Kr]$4d^2$, exhibits structures with approximate dodecahedral, D_{2d}, symmetry, as in $K_4Mo(CN)_8 \cdot 2H_2O$,[14−16] and square antiprismatic, D_{4d}, symmetry, as in $Tl_4Mo(CN)_8$.[17] Recent ab initio CASPT2 calculations indicate that the ground-state energies of these isolated polytopes differ by approximately 4 kcal mol^{-1},[18] with the D_{4d} form being the more stable of the two, and both being considerably lower than the cubic form.[19] In solution, the preferred stereochemical arrangement of cyanide ligands is an issue of debate. To this end, UV−vis,[20] Raman,[21−24] infrared,[22−25]

(1) Dunbar, K. R.; Heintz, R. A. *Prog. Inorg. Chem.* **1997**, *45*, 283−39.
(2) Withers, J. R.; Ruschmann, C.; Bojang, P.; Parkin, S.; Holmes, S. M. *Inorg. Chem.* **2005**, *44*, 352−358.
(3) Sokol, J. J.; Hee, A. G.; Long, J. R. *J. Am. Chem. Soc.* **2002**, *124*, 7656−7657.
(4) Hendrickx, M. F. A.; Clima, S.; Chibotaru, L. F.; Ceulemans, A. *J. Phys. Chem. A* **2005**, *109*, 8857−8864.
(5) Chibotaru, L. F.; Hendrickx, M. F. A.; Clima, S.; Larionova, J.; Ceulemans, A. *J. Phys. Chem. A.* **2005**, *109*, 7251−7257.
(6) Bennett, M. V.; Long, J. R. *J. Am. Chem. Soc.* **2003**, *125*, 2394−2395.
(7) Cotton, F. A.; Wilkinson, G.; Murillo, C. A.; Bochmann, M. *Advanced Inorganic Chemistry*, 6th ed.; Interscience Publishers: New York, 1999.
(8) Wells, A. F. *Structural Inorganic Chemistry*, 5th ed.; Oxford University Press: New York, 1984.
(9) Huheey, J. E.; Keiter, E. A.; Keiter, R. L. *Inorganic Chemistry − Principles of Structure and Reactivity*, 4th ed.; Harper Collins College Publishers: New York, 1993.
(10) Rosenheim, A. *Z. Anorg. Chem.* **1907**, *54*, 97−103.
(11) Leipoldt, J. G.; Basson, S. S.; Roodt, A. *Adv. Inorg. Chem.* **1993**, *40*, 241−322.
(12) Burdett, J. K.; Hoffmann, R.; Fay, R. C. *Inorg. Chem.* **1978**, *17*, 2553−2568.
(13) Muetterties, E. L.; Guggenberger, L. J. *J. Am. Chem. Soc.* **1974**, *96*, 1748−1756.
(14) Hoard, J. L.; Nordsieck, H. H. *J. Am. Chem. Soc.* **1939**, *61*, 2853−2863.
(15) Hoard, J. L.; Hamor, T. A.; Glick, M. D. *J. Am. Chem. Soc.* **1968**, *90*, 3177−3184.
(16) Mak, T. C. W.; Zhou, G.-D. *Crystallography in Modern Chemistry: A Resource Book of Crystal Structures*; John Wiley & Sons: New York, 1992.
(17) Meske, W.; Babel, D. *J. Alloys Compd.* **1992**, *183*, 158−167.
(18) Hendrickx, M. F. A.; Mironov, V. S.; Chibotaru, L. F.; Ceulemans, A. *Inorg. Chem.* **2004**, *43*, 3142−3150.
(19) Greenwood, N. N.; Earnshaw, A. *Chemistry of the Elements*; Pergamon Press: Oxford, 1984; Chapter 19.
(20) Perumareddi, J. R.; Liehr, A. D.; Adamson, A. W. *J. Am. Chem. Soc.* **1963**, *85*, 249−259.
(21) Parish, R. V.; Simms, P. G.; Wells, M. A.; Woodward, L. A. *J. Chem. Soc. A* **1968**, 2882−2886.

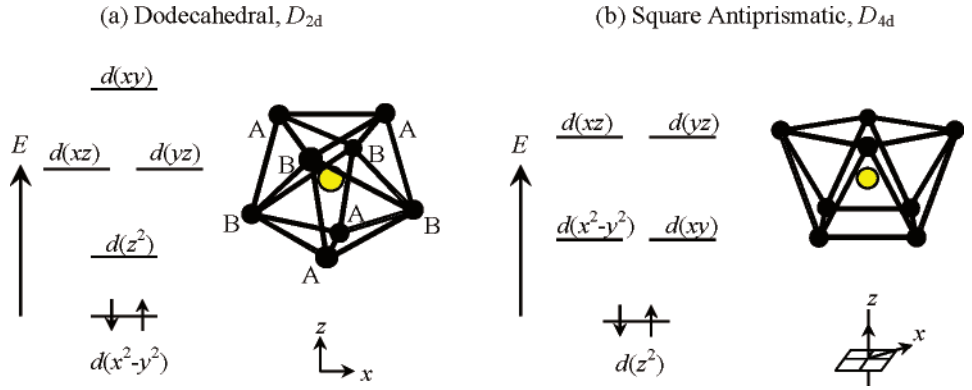

Figure 1. Idealized structural forms of the dodecahedral (a) and square antiprismatic (b) diamagnetic $Mo(CN)_8^{4-}$ anions.[12] For dodecahedral symmetry, the two types of cyanide ligands are labeled A and B, and for square antiprismatic symmetry, all cyanide ligands are equivalent due to the molecular symmetry. Partial electronic energy level diagrams for the $Mo(CN)_8^{4-}$ anions possessing ideal D_{2d} and D_{4d} symmetry are also shown. The ordering of molecular orbitals (MOs) corresponds to the orientation of the $Mo(CN)_8^{4-}$ anions in the indicated coordinate system, and the MO labels specify the dominant atomic orbital contributions localized on Mo.

and NMR[26−29] spectroscopic, as well as a variety of theoretical,[18,30,31] studies have been carried out to investigate the structure of $Mo(CN)_8^{4-}$ in solution. In addition, studies involving the electronic structure,[18,32,33] electron-transfer reactions,[34] electrochemistry,[35] and photomagnetic[36−38] properties of octacyanomolybdate, as well as applications toward molecular magnets,[2,39] continue to appear in the current literature.

Previous solution NMR studies consist of an early ^{13}C NMR study[26] of ^{13}C-enriched $K_4Mo(CN)_8 \cdot 2H_2O$ in aqueous solution and a variable-temperature ^{13}C NMR study[27] of $[N(n\text{-}C_3H_7)_4]_4Mo(CN)_8$ in a 90:10 $CHClF_2-CH_2Cl_2$ mixture. In the former study, a single carbon resonance was observed, and the authors addressed three possible explanations with the only realistic one being either the D_{4d} structure or D_{2d} with rapid intramolecular exchange of cyanide ligands.[26] The latter study[27] suggests a D_{2d} structure with rapid internal rearrangement of the two types of CN^- ligands via the concerted Hoard−Silverton pathway, facilitated by a low-energy barrier. Subsequent ^{95}Mo NMR studies[28,29] of $K_4Mo(CN)_8 \cdot 2H_2O$ in aqueous solutions concluded that the anion must possess D_{2d} symmetry since, based on the point-charge approximation (vide infra), the observed ^{95}Mo line widths of approximately 75 Hz are too large for compounds of cubic or square antiprismatic symmetry, where the electric field gradient, EFG, was expected to be zero. Similar conclusions were derived from ^{14}N and ^{95}Mo spin−lattice relaxation data, which indicated an effective ^{95}Mo quadrupolar coupling constant, C_Q, of approximately 3.6 MHz in aqueous solution.[29] A recent theoretical investigation seems to have ended the dispute on the symmetry of the anion in solution by concluding that a dynamic equilibrium between the D_{2d} and D_{4d} conformations must occur to account for all experimental bands in the electronic spectrum;[18] the interconversion between the two forms is facilitated by the small relative displacement of cyanide ligands (∼15°).[40]

The most thoroughly studied octacyanomolybdate is the K salt, $K_4Mo(CN)_8 \cdot 2H_2O$. Investigations of this compound in the solid state consist of ^{14}N NQR[41,42] and several single-crystal X-ray diffraction studies;[14−16] these studies indicate that there are six distinct cyanide ligands. No solid-state NMR studies of $K_4Mo(CN)_8 \cdot 2H_2O$ or any other octacyanomolybdate salt have been reported; however, the benefits of employing solid-state NMR are numerous. First, based on X-ray diffraction results,[14−17] the problems of molecular dynamics or interconversion between more than one symmetry form is not an issue in the solid state since the molecular structure is rigid, apart from molecular librations.[14−16] Second, solid-state NMR spectroscopy is ideally suited, in particular, for the Mo nucleus, because of the acute sensitivity of the Mo electric field gradient (EFG) and the magnetic shielding (σ) tensors to subtle changes in the local environment about Mo. Hence, undertaking separate studies of the approximate D_{2d} and D_{4d} symmetry forms of the $Mo(CN)_8^{4-}$ anion will allow proper characterization and a thorough understanding of their NMR parameters in the solid state, which may ultimately provide insight into results obtained in solution.

In the present study, diamagnetic octacyanomolybdate(IV) salts with approximate D_{2d} symmetry, $K_4Mo(CN)_8 \cdot 2H_2O$, and approximate D_{4d} symmetry, $Tl_4Mo(CN)_8$, have been examined using solid-state ^{95}Mo NMR spectroscopy at moderate (11.75 T) and high (17.63, 21.1 T) applied magnetic field strengths using the double-frequency sweep (DFS)[43] in combination with

(22) Edgar, K. *Theor. Chim. Acta* **1962**, *1*, 23−35.
(23) Stammreich, H.; Sala, O. *Z. Elektro. Angew. Phys. Chem.* **1961**, *65*, 149−150.
(24) Hartman, K. O.; Miller, F. A. *Spectrochim. Acta, Part A* **1968**, *24*, 669−684.
(25) Kettle, S. F. A.; Parish, R. V. *Spectrochim. Acta* **1965**, *21*, 1087−1093.
(26) Muetterties, E. L. *Inorg. Chem.* **1965**, *4*, 769−771.
(27) Muetterties, E. L. *Inorg. Chem.* **1973**, *12*, 1963−1966.
(28) Lutz, O.; Nolle, A.; Kroneck, P. *Z. Naturforsch., A: Phys. Sci.* **1976**, *31*, 454−456.
(29) Brownlee, R. T. C.; Shehan, B. P.; Wedd, A. G. *Inorg. Chem.* **1987**, *26*, 2022−2024.
(30) Gołębiewski, A.; Kowalski, H. *Theor. Chim. Acta* **1968**, *12*, 293−306.
(31) Gołębiewski, A.; Nalewajski, R. *Z. Naturforsch., A: Phys. Sci.* **1972**, *27*, 1672−1677.
(32) Hendrickx, M. F. A.; Chibotaru, L. F. Ceulemans, A. *Inorg. Chem.* **2003**, *42*, 590−597.
(33) Isci, H.; Mason, W. R. *Inorg. Chim. Acta* **2004**, *357*, 4065−4072.
(34) Yeow, E. K. L.; Slep, L. D.; Chibisov, A. K.; Braslavsky, S. E. *J. Phys. Chem. A* **2003**, *107*, 439−446; 2118.
(35) Schröder, U.; Scholz, F. *Inorg. Chem.* **2000**, *39*, 1006−1015.
(36) Ohkoshi, S.-I.; Tokoro, H.; Hozumi, T.; Zhang, Y.; Hashimoto, K.; Mathonière, C.; Bord, I.; Rombaut, G.; Verelst, M.; Cartier dit Moulin, C.; Villain, F. *J. Am. Chem. Soc.* **2006**, *128*, 270−277.
(37) Rombaut, G.; Verelst, M.; Golhen, S.; Ouahab, L.; Mathonière. C.; Kahn, O. *Inorg. Chem.* **2001**, *40*, 1151−1159.
(38) Mathonière, C.; Podgajny, R.; Guionneau, P.; Labrugere, C.; Sieklucka, B. *Chem. Mater.* **2005**, *17*, 442−449.
(39) Przychodzeń, P.; Lewiński, K.; Bałanda, M.; Pełka, R.; Rams, M.; Wasiutyński, T.; Guyard-Duhayon, C.; Sieklucka, B. *Inorg. Chem.* **2004**, *43*, 2967−2974.
(40) Sharpe, A. G. In *The Chemistry of Cyano Complexes of the Transition Metals*; Maitlis, P. M., Stone, F. G. A., West, R., Eds.; Academic Press: London, 1976; p 57.
(41) Murgich, J.; Bonalde, I.; Díaz, A.; Abanero, J. A. *J. Magn. Reson.* **1991**, *93*, 47−53.
(42) Murgich, J.; Oja, T. *J. Chem. Soc., Dalton Trans.* **1987**, 1637−1640.

the quadrupolar Carr−Purcell Meiboom−Gill (QCPMG)[44] experiment or simply the QCPMG experiment, and by computational means, employing the zeroth-order regular approximation density functional theory (ZORA DFT) and restricted Hartree−Fock (RHF) methods.

2. Background Theory

There are two NMR-active isotopes of molybdenum: ^{95}Mo and ^{97}Mo. Both are spin-$^5/_2$ quadrupolar nuclei with low NMR receptivities and moderate natural abundances (^{95}Mo: $\Xi = 6.547$ MHz, N.A. = 15.92%; ^{97}Mo: $\Xi = 6.685$ MHz, N.A. = 9.46%).[45] The preferred isotope for NMR studies is ^{95}Mo, since its nuclear quadrupole moment, $|Q|$, is an order of magnitude less than that for ^{97}Mo (^{95}Mo: $Q = -0.022 \times 10^{-28}$ m^2; ^{97}Mo: $Q = 0.17 \times 10^{-28}$ m^2).[45] Hundreds of solution ^{95}Mo NMR studies have been carried out, establishing a Mo chemical shift range of approximately 8000 ppm;[46] however, in the solid state, few NMR studies have been reported.[47−49,67,68] The lack of solid-state ^{95}Mo NMR studies is primarily due to the inherent difficulties associated with observing low-frequency quadrupolar nuclei. As well, the relatively small nuclear quadrupole moment of ^{95}Mo often leads to long spin−lattice relaxation times.[50] Despite these difficulties, such studies are becoming more common and feasible with the use of the highest possible magnetic field strengths (e.g., 21.1 and 17.63 T) and sensitivity-enhancement techniques (e.g., QCPMG, DFS/QCPMG). High magnetic fields result in increased sensitivity[51] and amplification of the magnetic shielding interaction, thus enabling more accurate determination of σ and the relative orientation of σ and EFG tensors. In addition, high magnetic fields substantially reduce probe ringing, which is often a problem when observing low-frequency quadrupolar nuclei.[51] The quality of the NMR experiments may be improved further, and a significant savings-in-time may be achieved with the use of sensitivity-enhancement techniques.

The NMR interactions of importance for ^{95}Mo in the octacyanomolybdate(IV) anions, under conditions where $\hat{\mathscr{H}}_Z \gg \hat{\mathscr{H}}_Q$, are the quadrupolar, $\hat{\mathscr{H}}_Q$, and magnetic shielding (chemical shift), $\hat{\mathscr{H}}_S$, interactions and are described in terms of the EFG and σ tensors, respectively. Detailed descriptions of the theories of the quadrupolar interaction and the nuclear magnetic shielding interaction have each been described elsewhere;[52−56] as well, examples characterizing the combined influence of these interactions on solid-state NMR spectra have been presented.[57−61] Herein, only the relevant parameters and conventions used will be presented.

To characterize the EFG tensor in its principal axis system (PAS), two parameters are required: the nuclear quadrupolar coupling constant, given in frequency units by $C_Q = eQV_{ZZ}/h$, where h is Planck's constant, and the asymmetry parameter, $\eta_Q = (V_{XX} - V_{YY})/V_{ZZ}$, with principal components of the EFG tensor ordered according to: $|V_{ZZ}| \geq |V_{YY}| \geq |V_{XX}|$. To describe the nuclear magnetic shielding, σ, in its PAS system, three parameters are required. The isotropic magnetic shielding, $\sigma_{iso} = (\sigma_{11} + \sigma_{22} + \sigma_{33})/3$, the anisotropic magnetic shielding or span, $\Omega = \sigma_{33} - \sigma_{11} = \delta_{11} - \delta_{33}$, and the skew, $\kappa = 3(\sigma_{iso} - \sigma_{22})/\Omega = 3(\delta_{22} - \delta_{iso})/\Omega$, which can take on values of -1 to $+1$, inclusive,[62] with principal components ordered according to: $\sigma_{33} \geq \sigma_{22} \geq \sigma_{11}$. Experimentally, the nuclear magnetic shielding is measured in relative terms using the chemical shift. Hence, for quadrupolar nuclei, where both $\hat{\mathscr{H}}_Q$ and $\hat{\mathscr{H}}_S$ are important, eight parameters must be determined: δ_{11}, δ_{22}, δ_{33}, C_Q, η_Q, and α, β, γ. The Euler angles, α, β, γ, define the relative orientation of the EFG and magnetic shielding tensors. The use of more than one applied magnetic field is generally required to analyze NMR spectra of stationary powder samples since, in frequency units, the second-order quadrupolar term, $\hat{\mathscr{H}}_Q$, depends on B_0^{-1}, whereas $\hat{\mathscr{H}}_S$ is directly proportional to B_0, thereby allowing the above parameters to be unambiguously determined.

For special symmetry cases, the EFG at a nucleus may be zero, or close to zero; this can be understood in terms of a rudimentary, but effective, theory known as the point-charge approximation (PCA). Using the PCA, the quadrupolar coupling can be estimated through the calculation of V_{ZZ} using:[63]

$$V_{ZZ} = \sum_i \frac{q_i}{4\pi\epsilon_0} \frac{(3\cos^2\theta_i - 1)}{r_i^3} \qquad (1)$$

where q_i is a charge at point (x_i, y_i, z_i), ϵ_0 is the free space permittivity, r_i is the distance from the point charge to the nucleus, and θ_i is the angle between vector r_i and the z-axis. From eq 1, it is straightforward to show that molecules possessing tetrahedral (T_d), octahedral (O_h), and square antiprismatic (D_{4d}) symmetry have a zero EFG at their center.[64] The geometrical constraint for a perfect tetrahedron, cube, or square antiprism is such that the angle formed between the

(43) Haase, J.; Conradi, M. S. *Chem. Phys. Lett.* **1993**, *209*, 287−291; Iuga, D.; Schäfer, H.; Verhagen, R.; Kentgens, A. P. M. *J. Magn. Reson.* **2000**, *147*, 192−209.
(44) Cheng, J. T.; Ellis, P. D. *J. Phys. Chem.* **1989**, *93*, 2549−2555; Larsen, F. H.; Skibsted, J.; Jakobsen, H. J.; Nielsen, Chr. N. *J. Am. Chem. Soc.* **2000**, *122*, 7080−7086.
(45) Harris, R. K.; Becker, E. D.; Cabral de Menezes, S. M.; Goodfellow, R.; Granger, P. *Encycl. Nuc. Magn. Reson.* **2002**, *9*, 5−19.
(46) Malito, J. *Ann. Rep. Nucl. Magn. Reson. Spectrosc.* **1997**, *33*, 151−206.
(47) Bryce, D. L.; Wasylishen, R. E. *Phys. Chem. Chem. Phys.* **2002**, *4*, 3591−3600.
(48) (a) Kautt, W. D.; Krüger, H.; Lutz, O.; Maier, H.; Nolle, A. *Z. Naturforsch., A: Phys. Sci.* **1976**, *31*, 351−356. (b) Mastikhin, V. M.; Lapina, O. B.; Maximovskaya, R. I. *Chem. Phys. Lett.* **1988**, *148*, 413−416. (c) Edwards, J. C.; Zubieta, J.; Shaikh, S. N.; Chen, Q.; Bank, S.; Ellis, P. D. *Inorg. Chem.* **1990**, *29*, 3381−3393. (d) Lynch, G. F.; Segel, S. L. *Can. J. Phys.* **1972**, *50*, 567−572.
(49) (a) Edwards, J. C.; Ellis, P. D. *Langmuir* **1991**, *7*, 2117−2134. (b) Edwards, J. C.; Adams, R. D.; Ellis, P. D. *J. Am. Chem. Soc.* **1990**, *112*, 8349−8364. (c) Edwards, J. C.; Ellis, P. D. *Magn. Reson. Chem.* **1990**, *28*, S59−S67.
(50) Bastow, T. J. *Solid State Nucl. Magn. Reson.* **1998**, *12*, 191−199.
(51) MacKenzie, K. J. D.; Smith, M. E. *Multinuclear Solid-State NMR of Inorganic Materials*; Pergamon Press: Amsterdam, 2002; Vol. 6, Chapter 8.
(52) Facelli, J. C.; Grant, D. M. *Top. Stereochem.* **1989**, *19*, 1−61.
(53) Samoson, A. *Chem. Phys. Lett.* **1985**, *119*, 29−32.
(54) Abragam, A. In *Principles of Nuclear Magnetism*; Adair, R. K., Elliott, R. J., Marshall, W. C., Wilkinson, D. H., Eds.; Clarendon Press: Oxford, 1961.
(55) (a) Haeberlen, U. In *Advances in Magnetic Resonance*; Waugh, J. S., Ed.; Academic Press: New York, 1976; Supplement 1, Chapter VI. (b) Anet, F. A. L.; O'Leary, D. J. *Concepts Magn. Reson.* **1991**, *3*, 193−214; Anet, F. A. L.; O'Leary, D. J. *Concepts Magn. Reson.* **1992**, *4*, 35−52.
(56) Veeman, W. S. *Prog. Nucl. Magn. Reson. Spectrosc.* **1984**, *16*, 193−235.
(57) Chu, P. J.; Gerstein, B. C. *J. Chem. Phys.* **1989**, *91*, 2081−2101.
(58) (a) Cheng, J. T.; Edwards, J. C.; Ellis, P. D. *J. Phys. Chem.* **1990**, *94*, 553−561. (b) Koons, J. M.; Hughes, E.; Cho, H. M.; Ellis, P. D. *J. Magn. Reson. A*, **1995**, *114*, 12−23.
(59) Bryce, D. L.; Eichele, K.; Wasylishen, R. E. *Inorg. Chem.* **2003**, *42*, 5085−5096.
(60) Power, W. P.; Wasylishen, R. E.; Mooibroek, S.; Pettitt, B. A.; Danchura, W. *J. Phys. Chem.* **1990**, *94*, 591−598.
(61) Bryce, D. L.; Eichele, K.; Wasylishen, R. E. *Inorg. Chem.* **2003**, *42*, 5085−5096.
(62) Mason, J. *Solid State Nucl. Magn. Reson.* **1993**, *2*, 285−288.
(63) Slichter, C. P. In *Principles of Magnetic Resonance*, 3rd enlarged and updated edition; Fulde, P., Ed.; Springer-Verlag: Berlin, 1990; p 502.
(64) Han, O. H.; Oldfield, E. *Inorg. Chem.* **1990**, *29*, 3666−3669.

ligand, metal center, and principal molecular axis must be equal to the magic angle, ~54.74°; for such cases, V_{ZZ} is simply zero.[65,66] It is important to stress that the square antiprism is a special case of D_{4d} symmetry; any deviation of θ_i from the magic angle will result in a structure which, although may retain D_{4d} symmetry, no longer sustains the essential square antiprismatic symmetry that results in a zero EFG at Mo, according to the PCA. Experimentally, however, structural deviations from ideal symmetry, whether square antiprismatic, tetrahedral, or octahedral, often result in small, measurable EFGs, i.e., C_Q's. For example, the observed $C_Q(^{95}Mo)$ values for a series of molybdate salts vary from 0.34 to 3.08 MHz, depending on the extent of distortion from T_d symmetry.[67,68] Nonetheless, based on the PCA, the $Mo(CN)_8^{4-}$ anions possessing approximate dodecahedral and square antiprismatic symmetry should result in ^{95}Mo NMR spectra that are significantly different, allowing the two structures to be easily distinguished.

3. Experimental and Computational Details

3.1. Nuclear Magnetic Resonance Spectroscopy. Samples of $K_4Mo(CN)_8 \cdot 2H_2O$ were either purchased from Aldrich and used without further purification or synthesized[69] according to literature procedures; $Tl_4Mo(CN)_8$ was synthesized according to a literature procedure.[17] The samples were powdered and packed into 5.0 mm glass NMR tubes or 7.0 mm o.d. ZrO_2 rotors. Solid-state ^{95}Mo NMR experiments were performed on Bruker Avance (11.75 T) and Varian Inova (17.63 and 21.1 T) spectrometers, operating at spectral frequencies of 32.55, 48.68, and 58.57 MHz, respectively, and using double-resonance MAS probes. The accepted Mo chemical shift reference,[45] a 2.0 M aqueous solution of $Na_2MoO_4 \cdot 2H_2O$ ($\delta_{iso} = 0$ ppm), was used for referencing and pulse width calibration. Employing a standard one-pulse experiment, typical solution $\pi/2$ pulse widths of 6.0−10.3 μs were obtained. The QCPMG pulse sequence, $(\pi/2)_x-\tau_1-\pi_y-\tau_2-(\tau_a/2)-[\tau_3-\pi_y-\tau_4-\tau_a]_M-\tau_d$, was used to acquire ^{95}Mo NMR spectra of $K_4Mo(CN)_8 \cdot 2H_2O$ at 11.75 and 17.63 T and $Tl_4Mo(CN)_8$ at 11.75 T, while the combined DFS/QCPMG experiment was used to collect ^{95}Mo NMR spectra of $Tl_4Mo(CN)_8$ at 21.1 T. Spectral sweep widths of 100 kHz were employed at 11.75 T, 500 kHz at 17.63 T, and 1.0 MHz at 21.1 T. Acquisition times of 25−65 ms, solid selective $\pi/2$ pulse widths, [(solution $\pi/2$)/($I + {}^1/_2$)], of 2.0−3.4 μs, pulse delays of 8−10 s and pulse train repetitions, M, of 32−48 were used. High-power ^1H decoupling was used for $K_4Mo(CN)_8 \cdot 2H_2O$ at 11.75 T. The spin−echo delays, τ_1, τ_2, τ_3, and τ_4, varied between 80 μs and 110 μs and are used to minimize effects from probe ringing. The spikelet spacing, ν_{QCPMG}, equal to τ_a^{-1}, where τ_a is the acquisition time for a complete echo, was 500 Hz for the K salt at 17.63 T, 500 Hz for the Tl salt at 21.1 T, and 1940 Hz for the K and Tl salts at 11.75 T. For ^{95}Mo NMR spectra of $Tl_4Mo(CN)_8$ acquired at 21.1 T using the DFS/QCPMG pulse sequence, the DFS pulse was 1.0 ms with low and high offsets of 1.0 MHz and 100 kHz, respectively.

Attempts at acquiring ^{95}Mo QCPMG NMR spectra of magic-angle spinning (MAS) samples of $K_4Mo(CN)_8 \cdot 2H_2O$ and $Tl_4Mo(CN)_8$ at 11.75 T were unsuccessful due to insufficient rotor spinning speeds for 7.0 mm rotors.

Solid-state ^{13}C NMR spectra of $K_4Mo(CN)_8 \cdot 2H_2O$ and $Tl_4Mo(CN)_8$ were collected on a Bruker Avance 500 ($B_0 = 11.75$ T; $\nu_L(^{13}C) = 125.8$ MHz) spectrometer; high−power ^1H decoupling was used for the K salt. Samples of solid $K_4Mo(CN)_8 \cdot 2H_2O$ and $Tl_4Mo(CN)_8$ were powdered and packed into 7.0 mm and 4.0 mm o.d. ZrO_2 rotors, respectively. Due to the anticipated long ^{13}C spin−lattice relaxation times for solid $K_4Mo(CN)_8 \cdot 2H_2O$ and $Tl_4Mo(CN)_8$, 45° flip angles corresponding to pulse widths of 2.75 and 3.00 μs, respectively, and unoptimized pulse delays of 600 s were used to avoid saturation of the magnetization. Sweep widths of 100 kHz and spinning frequencies of 6.8 kHz and 12.0 kHz were used for the K and Tl salts, respectively.

Simulations of ^{95}Mo and ^{13}C NMR spectra of $K_4Mo(CN)_8 \cdot 2H_2O$ and $Tl_4Mo(CN)_8$ were carried out using SIMPSON[70] or WSOLIDS.[71]

3.2. Quantum Chemical Calculations. Nonrelativistic and spin−orbit relativistic ZORA DFT calculations of molybdenum and carbon magnetic shielding and molybdenum EFG tensors for isolated octacyanomolybdate(IV) anions possessing D_{2d} and D_{4d} symmetry were performed using the NMR module[72] of the Amsterdam Density Functional program.[73,74] The Vosko−Wilk−Nusair (VWN) local density approximation[75] with the Becke[76]−Perdew[77] generalized gradient approximation (GGA) were used for the exchange-correlation functional. Relativistic calculations included scalar + spin−orbit corrections and were carried out using the ZORA formalism.[78−82] The quadruple-ζ quadruply polarized (QZ4P) or double-ζ (DZ) Slater-type ZORA basis sets, available with the ADF program, were employed for Mo, C, and N.

ZORA DFT calculations of EFG[83] and magnetic shielding tensors were performed on the isolated $Mo(CN)_8^{4-}$ anion using experimental structures determined from single-crystal X-ray diffraction studies[14−17] (C_s symmetry for the K salt and C_1 symmetry for the Tl salt); as well, analogous calculations on idealized structures of $Mo(CN)_8^{4-}$ possessing D_{2d} and square antiprismatic symmetry were carried out. The molecular coordinates used for the idealized $Mo(CN)_8^{4-}$ anions are included in Supporting Information. In addition, a calculation carried out at the nonrelativistic level employing ZORA DZ basis sets was performed on $Tl_4Mo(CN)_8$ by including the first coordination sphere of four Tl cations, i.e., within a distance of 4.85 Å from Mo, to test the effects of inclusion of the Tl cations on the Mo EFG and magnetic shielding tensors. Further Mo EFG and magnetic shielding tensor calculations were carried out on isolated molybdenum-containing anions and compounds possessing T_d or O_h symmetry: MoO_4^{2-},[84] MoS_4^{2-},[85] $MoSe_4^{2-}$,[86] and $Mo(CO)_6$,[87] to establish the accuracy of the calculated molybdenum magnetic shielding (chemical shift) scale and to compare EFGs calculated using quantum chemistry computations with those determined using the PCA. Last, nonrelativistic ZORA DFT calculations

(65) Akitt, J. W.; McDonald, W. S. *J. Magn. Reson.* **1984**, *58*, 401−412.
(66) Akitt, J. W. *Prog. Nucl. Magn. Reson. Spectrosc.* **1989**, *21*, 1−149.
(67) Eichele, K.; Wasylishen, R. E.; Nelson, J. H. *J. Phys. Chem. A* **1997**, *101*, 5463−5468.
(68) d'Espinose de Lacaillerie, J.-B.; Barberon, F.; Romanenko, K. V.; Lapina, O. B.; Le Pollès, L.; Gautier, R.; Gan, Z. *J. Phys. Chem. B* **2005**, *109*, 14033−14042.
(69) Leipoldt, J. G.; Bok, L. D. C.; Cilliers, P. J. *Z. Anorg. Allg. Chem.* **1974**, *407*, 350−352.
(70) Bak, M.; Rasmussen, J. T.; Nielsen, N. C. *J. Magn. Reson.* **2000**, *147*, 296−330.
(71) Eichele, K.; Wasylishen, R. E. *WSOLIDS NMR Simulation Package*, Version 1.17.26; 2000.
(72) (a) Schreckenbach, G.; Ziegler, T. *Int. J. Quantum Chem.* **1997**, *61*, 899−918. (b) Wolff, S. K.; Ziegler, T. *J. Chem. Phys.* **1998**, *109*, 895−905.
(73) ADF 2000.02, 2002.99, and 2004.01, *Theoretical Chemistry*; Vrije Universiteit: Amsterdam, http://www.scm.com.
(74) (a) Baerends, E. J.; Ellis, D. E.; Ros, P. *Chem. Phys.* **1973**, *2*, 41−51. (b) Versluis, L.; Ziegler, T. *J. Chem. Phys.* **1988**, *88*, 322−328. (c) te Velde, G.; Baerends, E. J. *J. Comput. Phys.* **1992**, *99*, 84−98. (d) Fonseca Guerra, C.; Snijders, J. G.; te Velde, G.; Baerends, E. J. *Theor. Chem. Acc.* **1998**, *99*, 391−403.
(75) Vosko, S. H.; Wilk, L.; Nusair, M. *Can. J. Phys.* **1980**, *58*, 1200−1211.
(76) Becke, A. D. *Phys. Rev. A* **1988**, *38*, 3098−3100.
(77) Perdew, J. P. *Phys. Rev. B* **1986**, *33*, 8822−8824; Perdew, J. P. *Phys. Rev. B* **1986**, *34*, 7406−7406.
(78) Chang, C.; Pelissier, M.; Durand, P. *Phys. Scr.* **1986**, *34*, 394−404.
(79) van Lenthe, E.; Baerends, E. J.; Snijders, J. G. *J. Chem. Phys.* **1993**, *99*, 4597−4610.
(80) van Lenthe, E.; Baerends, E. J.; Snijders, J. G. *J. Chem. Phys.* **1994**, *101*, 9783−9792.
(81) van Lenthe, E.; Ehlers, A.; Baerends, E. J. *J. Chem. Phys.* **1999**, *110*, 8943−8953.
(82) van Lenthe, E.; van Leeuwen, R.; Baerends, E. J.; Snijders, J. G. *Int. J. Quantum Chem.* **1996**, *57*, 281−293.
(83) van Lenthe, E.; Baerends, E. J. *J. Chem. Phys.* **2000**, *112*, 8279−8292.
(84) Matsumoto, K.; Kobayashi, A.; Sasaki, Y. *Bull. Chem. Soc. Jpn.* **1975**, *48*, 1009−1013.
(85) Kanatzidis, M. G.; Coucouvanis, D. *Acta Crystallogr., Sect. C* **1988**, *39*, 835−838.
(86) O'Neal, S. C.; Kolis, J. W. *J. Am. Chem. Soc.* **1988**, *110*, 1971−1973.
(87) Mak, T. C. W. *Z. Kristallogr.* **1984**, *166*, 277−281.

of the Mo EFG tensors were carried out on a series of isolated, idealized anions possessing D_{4d} symmetry, as well as various rotamers of Mo(CN)$_8^{4-}$ including O_h symmetry. The hypothetical Mo(CN)$_8^{4-}$ anion possessing O_h symmetry, i.e., a cube, was generated from that possessing D_{4d} symmetry by rotating the upper portion of the square antiprism with respect to the bottom portion by 45°. A total of nine rotamers were subsequently generated by rotating the upper portion of the O_h structure in increments of 5° until the square antiprismatic structure was restored (D_{4d} symmetry retained). The ZORA DZ basis sets were used for all atoms, except the calculation on the O_h rotamer, for which ZORA QZ4P basis sets were used due to convergence problems when using ZORA DZ basis sets.

Idealized structures were generated using the average bond lengths and bond angles from the crystal structures, while ensuring that the symmetry operations of the appropriate point groups (T_d, O_h, D_{2d}, and D_{4d}) were obeyed. For D_{2d} symmetry, two types of CN^- ligands (A and B) were generated (Figure 1). For all calculations, the molecules were oriented with Mo at the origin and the principal molecular axes along the *z*-axis.

Calculated isotropic Mo magnetic shielding values were converted to calculated isotropic chemical shift values by first setting the calculated chemical shift value of $Mo(CO)_6$ to its accepted experimental value, $\delta(\text{ref})_{\text{iso,calc}} = -1860$ ppm, and subsequently converting the calculated $\sigma_{\text{iso,calc}}$ values for the remaining Mo compounds to $\delta_{\text{iso,calc}}$ using: $\delta(\text{sample})_{\text{iso,calc}} \approx \sigma(\text{ref})_{\text{iso,calc}} - \sigma(\text{sample})_{\text{iso,calc}} - 1860$ ppm.

To determine contributions from the paramagnetic shielding, σ_{para}, to the principal components of the Mo magnetic shielding tensor, nonrelativistic ZORA DFT calculations were carried out using the EPR module[88] of the ADF program. Calculations were performed on isolated, idealized, closed-shell D_{2d} and D_{4d} Mo(CN)$_8^{4-}$ anions using DZ basis sets for all atoms.

Calculations of the Mo EFG tensor were repeated at the restricted Hartree−Fock (RHF) level of theory using Parallel Quantum Solutions[89] and MOLOPRO.[90] RHF calculations were carried out on the isolated D_{4d} Mo(CN)$_8^{4-}$ anion as well as the aforementioned rotamers (O_h symmetry through to square antiprismatic D_{4d} symmetry in 5° increments). In all RHF calculations, the minimal 3-21G basis set was employed for Mo due to a limited basis set selection. Nuclear quadrupolar coupling constants were subsequently calculated (in frequency units) using $C_Q = eQV_{ZZ}/h$. Conversion of V_{ZZ} from atomic units to V m^{-2} was carried out using the factor, 9.717 36 × 10^{21} V m^{-2} per atomic unit.[91]

Point-charge calculations of V_{ZZ} were carried out on models possessing T_d, O_h, and D_{4d} symmetry using eq 1. The atomic charges for Mo, C, N, and O were taken from spin−orbit relativistic ZORA DFT calculations using QZ4P basis sets.

4. Results and Discussion

4.1. $K_4Mo(CN)_8\cdot 2H_2O$: Approximate Dodecahedral Symmetry. Shown in Figure 2 are solid-state ^{95}Mo QCPMG NMR spectra of stationary, powdered samples of $K_4Mo(CN)_8\cdot 2H_2O$ acquired at 11.75 and 17.63 T, along with their best-fit simulated spectra; the best-fit parameters are listed in Table 1. The separation between spikelets, ν_{QCPMG}, 1940 and 500 Hz at 11.75 and 17.63 T, respectively, provides a well-defined ^{95}Mo NMR line shape and adequate S/N. In addition, the relative breadths of the ^{95}Mo NMR spectra illustrate the benefits of employing higher magnetic fields due to the inverse scaling of the second-order quadrupolar interaction with B_0. Assuming the quadrupolar interaction is the only important internal interaction, the breadth of the NMR line shape for a quadrupolar nucleus acquired at 17.63 T is roughly 1.5 times narrower in frequency units than that at 11.75 T. However, upon inspection of Figure 2, the observed breadth of the ^{95}Mo NMR spectrum of $K_4Mo(CN)_8\cdot 2H_2O$ acquired at 17.63 T (10.5 kHz) appears to be approximately one-fourth the breadth (one-third in Hz) of that at 11.75 T (32.5 kHz). The difference in the ratio must arise from the magnitude of the Mo magnetic shielding tensor and the relative orientation of the EFG and magnetic shielding tensors (vide infra).

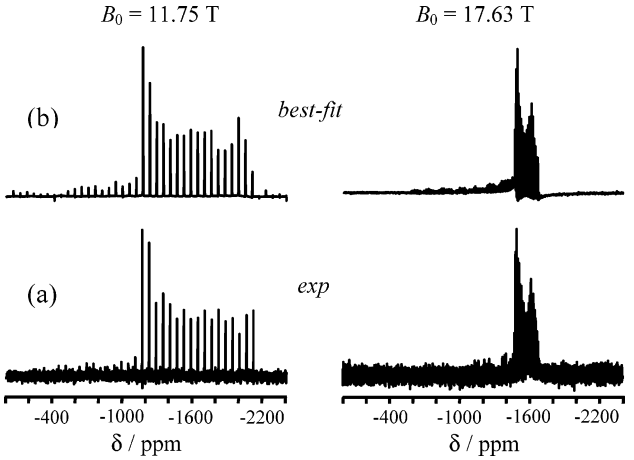

Figure 2. Experimental (a) and best-fit simulated (b) QCPMG ^{95}Mo central transition NMR spectra of a solid stationary sample of $K_4Mo(CN)_8\cdot 2H_2O$ acquired at 11.75 T (left) and 17.63 T (right). The parameters used to calculate the simulated spectra are given in Table 1. A total of 24 682 and 4480 transients were summed for spectra acquired at 11.75 and 17.63 T, respectively. An expansion of the experimental and simulated QCPMG spectra acquired at 17.63 T is given in the Supporting Information.

To aid in interpreting the ^{95}Mo NMR spectra, it is useful to refer to X-ray diffraction data. $K_4Mo(CN)_8\cdot 2H_2O$ crystallizes in space group *Pnma*, and the anion is approximately described by D_{2d} symmetry. For ideal D_{2d} symmetry, there are two perpendicular mirror planes, resulting in two crystallographically distinct cyanide ligands, labeled A and B in Figure 1. In contrast, the experimental structure possesses a single mirror plane, in which Mo and four carbon atoms (two C_A and two C_B) lie, resulting in six crystallographically unique carbon atoms; hence, the actual point group symmetry of the experimental anion is C_s.[15] Our ^{13}C NMR spectrum of an MAS sample of $K_4Mo(CN)_8\cdot 2H_2O$ (not shown) reveals six resolved ^{13}C signals, in agreement with both X-ray[14−16] and ^{14}N NQR[41,42] data. The small deviation from D_{2d} symmetry is apparent from the near axially-symmetric Mo EFG and magnetic shielding tensors (Table 1) and carbon magnetic shielding tensors.

Shown in Figure 3 are the individual contributions from the Mo magnetic shielding and EFG tensors to the ^{95}Mo NMR spectra of $K_4Mo(CN)_8\cdot 2H_2O$ determined from the best-fit experimental parameters in Table 1. At the fields employed here, the anisotropic Mo magnetic shielding makes approximately equal contributions to the ^{95}Mo central transition NMR spectra as the quadrupolar interaction—a common occurrence for heavy nuclei with large chemical shift ranges, such as Mo. The experimental quadrupolar coupling constant, $C_Q = (-)7.08$ MHz, is approximately twice that deduced from solution ^{14}N and ^{95}Mo T_1 measurements, $C_Q = 3.61$ MHz.[29] Since the sign

(88) Schreckenbach, G.; Ziegler, T. *J. Phys. Chem.* **1995**, *99*, 606−611.
(89) *PQS*, Version 2.5; Parallel Quantum Solutions: Fayetteville, AK; http://www.pqs-chem.com. sales@pqs-chem.com
(90) *MOLPRO*, a package of ab initio programs; Werner, H.-J.; Knowles, P. J.; Lindh, R.; Schütz, M.; and others; version 2002.6100.
(91) Mills, I.; Cvitaš, T.; Homann, K.; Kallay, N.; Kuchitsu, K. *Quantities, Units and Symbols in Physical Chemistry*, 2nd ed.; Blackwell Science: Oxford, 1993.

Table 1. Experimental and Calculated Mo σ and EFG Parameters for $K_4Mo(CN)_8 \cdot 2H_2O$

δ_{iso}/ppm[a]	Ω/ppm	κ	C_Q/MHz	η_Q	α, β, γ/°
		Experimental: Solid-State ^{95}Mo NMR			
-1322 ± 5	1160 ± 30	-0.987 ± 0.013	$(-)7.08 \pm 0.05$	0.065 ± 0.030	$0 \pm 30, 90, 0$
		Calculated:[b] Scalar + Spin−Orbit Relativistic			
−1223[c]	971	−0.996	−7.08	0.027	88, 90, 0
		Calculated:[b] Nonrelativistic			
−1186[d]	1016	−0.928	−7.32	0.026	122, 90, 177
		Calculated: Nonrelativistic (Ideal D_{2d} $Mo(CN)_8^{4-}$ anion)			
−1212	993	−1.00	−7.47	0.00	NA,[e] 90, 0

[a] Calculated isotropic chemical shifts were determined using $\delta(\text{ref})_{iso,calc} = -1860.0$ ppm for $Mo(CO)_6$ and $\delta(\text{sample})_{iso,calc} - \delta(\text{ref})_{iso,calc} \approx \sigma(\text{ref})_{iso,calc} - \sigma(\text{sample})_{iso,calc}$. [b] ZORA DFT calculations using QZ4P basis sets were performed on the isolated $Mo(CN)_8^{4-}$ anion using coordinates as determined from single-crystal X-ray structure data. [c] Spin−orbit: for $Mo(CO)_6$, $\sigma(\text{ref})_{iso,calc} = 1572.3$ ppm and $\delta(\text{ref})_{iso,calc} = -1860$ ppm. [d] Nonrelativistic: for $Mo(CO)_6$, $\sigma(\text{ref})_{iso,calc} = 1229.4$ ppm and $\delta(\text{ref})_{iso,calc} = -1860$ ppm. [e] Due to the axial symmetry of the CS and EFG tensors, the calculated line shape for the ^{95}Mo NMR spectrum is invariant to angle, α.

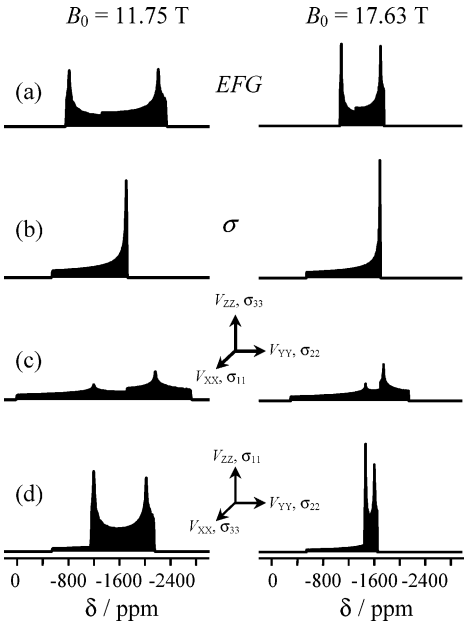

Figure 3. Simulations of central transition ^{95}Mo NMR spectra of solid, stationary $K_4Mo(CN)_8 \cdot 2H_2O$ to show the individual contributions from the EFG (a) and σ (b) interactions. The sum of these interactions is shown in (c, d) using two possible relative orientations of the EFG and σ tensors. Simulations which best match the experimental spectra are shown in (a), and the corresponding best-fit simulation parameters are given in Table 1.

of C_Q(^{95}Mo) for $K_4Mo(CN)_8 \cdot 2H_2O$ cannot be determined from ^{95}Mo NMR experiments, it is inferred from our DFT calculations and assumed to be correct, given the accuracy of the magnitude of the calculated C_Q values. The anisotropic Mo magnetic shielding tensor spans 1160 ppm and is among the largest reported[47] for a Mo compound. The isotropic Mo chemical shift, $\delta_{iso} = -1322 \pm 5$ ppm, for solid $K_4Mo(CN)_8 \cdot 2H_2O$ indicates that the Mo is shielded by 14 ppm compared to that for an aqueous solution of $K_4Mo(CN)_8 \cdot 2H_2O$, −1308 ppm.[92] The observed line shape and breadth of the ^{95}Mo NMR spectrum is highly sensitive to the orientation of the principal components of the Mo EFG and magnetic shielding tensor, as well as their relative orientation. The crystallographic mirror plane in $K_4Mo(CN)_8 \cdot 2H_2O$ restricts the relative orientation of the Mo σ and EFG tensors: one component of each of the tensors must lie perpendicular to this plane, and the remaining two components must lie in the plane. Recognizing that the only possible orientation for the largest, and unique, component of the EFG tensor, V_{ZZ}, is perpendicular to the mirror plane leaves the orientation of the magnetic shielding tensor to be determined. Given that σ has near axial symmetry, $\kappa = -0.987$, either σ_{11} or σ_{33} must be colinear with V_{ZZ}. Shown in Figure 3, c and d, are two possible relative orientations of the EFG and σ tensors. From these simulations, the only orientation consistent with experiment is that where V_{ZZ} and σ_{11} are co−linear and perpendicular to the mirror plane; hence, $\beta = 90°$ and $\gamma = 0°$ (Figure 3d). This orientation, in combination with the magnitudes of the Mo σ and EFG tensors, explains the apparent squeezing of the spectrum at 17.63 T and the origin of the low-intensity spikelets on the high frequency side of the powder pattern, which are barely discernible from the noise. Although these peaks are weak, they are present in all experiments and occur at the expected spacing, ν_{QCPMG}. The remaining Euler angle, α, is not restricted by the crystal symmetry and was determined by systematically varying the angle and visually comparing the resultant simulated spectrum with experiment; values of $\alpha = 0 \pm 30°$ were found to provide a good fit with the experimental spectra.

To help rationalize the significant EFG and large observed Mo magnetic shielding anisotropy for $K_4Mo(CN)_8 \cdot 2H_2O$, relativistic and nonrelativistic ZORA DFT computations of the Mo magnetic shielding and EFG tensors were carried out on the isolated $Mo(CN)_8^{4-}$ anion[93] using the experimental X-ray structure. The calculated results are given in Table 1, and despite our calculations being carried out on the isolated anion, $Mo(CN)_8^{4-}$, the results are in good agreement with experiment. Although results for the isotropic magnetic shielding values using spin−orbit relativistic and nonrelativistic calculations differ by several hundred ppm, their respective *chemical shift* values are in good agreement with experiment. In addition, values for Ω, κ, C_Q, and η_Q are similar for the spin−orbit relativistic and nonrelativistic values.

For comparison, calculations of the Mo magnetic shielding and EFG tensors were also carried out on the $Mo(CN)_8^{4-}$ anion with imposed D_{2d} symmetry and results obtained from nonrelativistic DFT calculations are summarized in Table 1. As expected, the Mo magnetic shielding and EFG tensors for ideal D_{2d} symmetry are axially symmetric, and differences in the magnitudes of these tensors between the idealized D_{2d} model and the experimental structure are minor. Still, the calculated

(92) Lutz, O.; Nolle, A.; Kroneck, P. *Z. Naturforsch., A: Phys. Sci.* **1977**, *32*, 505−506.

(93) Calculations were performed with Mo at the origin and the formal C_2-axis aligned parallel to the *z*-axis.

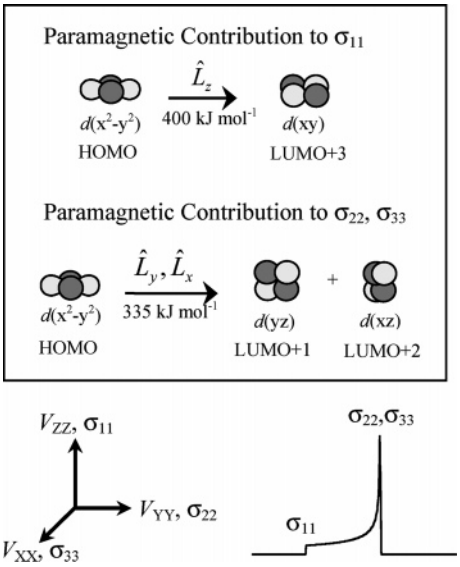

Figure 4. Origin of the paramagnetic shielding contribution to the principal components of the Mo magnetic shielding tensor, σ_{ii}^{para}, for D_{2d} Mo(CN)$_8^{4-}$ as determined by our DFT calculations. Symmetry-allowed mixing between occupied and virtual Mo d-dominated molecular orbitals via the orbital angular momentum operators, $\hat{L}_x$, $\hat{L}_y$, and $\hat{L}_z$ give rise to σ_{ii}^{para}. The relative orientation of the Mo σ and EFG tensors in the molecular frame (i.e., V_{XX}, V_{YY}, and V_{ZZ} are coincident with the *x*-, *y*-, *z*-axes), along with the Mo σ powder pattern, is shown to help visualize and rationalize the mixing of orbitals.

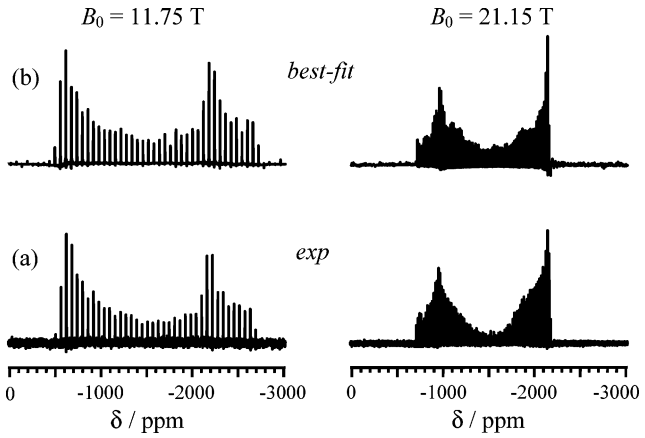

Figure 5. Experimental (a) and best-fit simulated (b) ^{95}Mo central transition NMR spectra of a solid stationary sample of $Tl_4Mo(CN)_8$ acquired using the QCPMG pulse sequence at 11.75 T (left) and the DFS/QCPMG pulse sequence at 21.15 T (right). The parameters used to calculate the simulated spectra are given in Table 2. A total of 31 760 transients were summed for $Tl_4Mo(CN)_8$ at 11.75 T and 8192 at 21.15 T.

results for ideal D_{2d} Mo(CN)$_8^{4-}$ are useful in providing insight into the origin of the large observed and calculated Mo magnetic shielding anisotropy. The magnetic shielding is governed by the paramagnetic shielding term,[94] which operates via mixing of occupied and virtual molecular orbitals (MOs) of appropriate symmetry that are centered on the nucleus of interest. Hence, inspection of the energy level diagram (Figure 1a) and the contribution of atomic orbitals to the MOs is required to understand the magnetic shielding for D_{2d} Mo(CN)$_8^{4-}$. Examination of our ZORA DFT calculations for ideal D_{2d} Mo(CN)$_8^{4-}$ indicates that the HOMO, as well as many low-lying virtual orbitals, are dominated by Mo d orbitals. The ordering of selected energy levels for D_{2d} Mo(CN)$_8^{4-}$ (Figure 1a) is in agreement with that determined by others.[18,95−97] In addition to the MOs, the magnitude and orientation of the Mo magnetic shielding tensor in the molecular frame must be considered. For D_{2d} symmetry there are two unique magnetic shielding tensor components, σ_{11} and $\sigma_{22} = \sigma_{33}$, referring to the magnetic shielding components oriented perpendicular and parallel to the molecular *z*-axis, respectively. Since the unique component of the Mo magnetic shielding tensor for D_{2d} Mo(CN)$_8^{4-}$, σ_{11}, is oriented along the molecular *z*-axis, orbitals contributing to σ_{11} must lie in the *xy*-plane and the symmetry-allowed mixing of these orbitals occurs via rotation about the *z*-axis. According to our calculations on ideal D_{2d} Mo(CN)$_8^{4-}$, the most plausible source of the large paramagnetic contribution to σ_{11} is mixing of occupied d(x^2-y^2) and unoccupied d(*xy*) orbitals via the *z*-component of the orbital angular momentum operator, $\hat{L}_Z$, as mixing of these orbitals is symmetry allowed,[98] and their energy difference is small (Figure 4). Mixing of d(x^2-y^2) and d(*xy*) occurs between several MOs and each makes a substantial contribution to σ_{11}^{para}; the most substantial contribution involves mixing of the HOMO with the LUMO+12, LUMO+3, and LUMO+13. In this case, the largest contribution of the paramagnetic term is governed by the most favorable overlap, rather than the smallest energy gap. Mixing of the orbitals in the *xy* plane via $\hat{L}_Z$ only influences the shielding component along the *z*-axis; furthermore, rotations which affect σ_{11} do not affect $\sigma_{22} = \sigma_{33}$ and vice versa. Since the d(*xz*) and d(*yz*) orbitals are degenerate, rotations involving d(x^2-y^2) via $\hat{L}_y$ or $\hat{L}_x$ result in contributions to the paramagnetic shielding of σ_{22} and σ_{33} (Figure 4). This mixing involves the HOMO, d(x^2-y^2), with each of the following degenerate pairs of d(*xz*) or d(*yz*) dominated virtual orbitals: LUMO+1, +2, LUMO+5, +6, and LUMO+9, +10. For comparison, the difference in the total paramagnetic shielding between σ_{11} and $\sigma_{22} = \sigma_{33}$ is 933 ppm, whereas the difference in the total diamagnetic shielding between σ_{11} and $\sigma_{22} = \sigma_{33}$, 12 ppm, is negligible. Together, the total diamagnetic and paramagnetic contributions result in a large deshielding of the principal components for ideal D_{2d} Mo(CN)$_8^{4-}$, $\sigma_{iso} = 936$ ppm (spin−orbit relativistic; Table 1), with respect to the bare nucleus, $\sigma_{iso} \approx 4317.7$ ppm.[99]

4.2. $Tl_4Mo(CN)_8$: Approximate Square Antiprismatic Symmetry. Shown in Figure 5 are experimental and best-fit simulated solid-state ^{95}Mo QCPMG (11.75 T) and DFS/QCPMG (21.1 T) NMR spectra of a stationary sample of $Tl_4Mo(CN)_8$, possessing approximate D_{4d} symmetry. The parameters used to calculate the best-fit ^{95}Mo NMR spectra (Figure 5b) are listed in Table 2. The separation between spikelets is approximately 1940 Hz at 11.75 T and 500 Hz at 21.1 T. These spectra immediately suggest that structural deviations in the Mo(CN)$_8^{4-}$ anion from square antiprismatic symmetry must be significant since, according to the PCA, a null EFG at Mo is predicted for

(94) (a) Ramsey, N. F. *Phys. Rev.* **1950**, *77*, 567 (b) Jameson, C. J. In *Multinuclear NMR*; Mason, J., Ed., Plenum Press: New York, 1987; Chapter 3.
(95) Golding, R. M. *Applied Wave Mechanics*; D. Van Nostrand: London, 1969.
(96) Corden, B. J.; Cunningham, J. A.; Eisenberg, R. *Inorg. Chem.* **1970**, *9*, 356−362.
(97) Golding, R. M.; Carrington, A. *Mol. Phys.* **1962**, 377−385.
(98) Jameson, C. J.; Gutowsky, H. S. *J. Chem. Phys.* **1964**, *40*, 1714−1724.
(99) This value for σ_{iso}(Mo), 4317 ppm, was extrapolated from a plot of σ_{iso}(calc) vs atomic number for all closed-shell atoms. Calculations were performed using spin−orbit relativistic ZORA DFT. This extrapolation method was employed because the program ADF does not yet permit shielding calculations on open-shell systems.

Table 2. Experimental and Calculated Mo σ and EFG Parameters for $Tl_4Mo(CN)_8$

δ_{iso}/ppm[a]	Ω/ppm	κ	C_Q/MHz	η_Q	α, β, γ/°
		Experimental: Solid-State ^{95}Mo NMR			
-1350 ± 10	1350 ± 30	$+0.50 \pm 0.05$	$+6.35 \pm 0.15$	0.50 ± 0.08	$90 \pm 5, 0, 0$
		Calculated:[b] Scalar + Spin−Orbit Relativistic			
−1308[c]	989	+0.50	+6.34	0.86	92, 171, 9
		Calculated:[b] Nonrelativistic			
−1273[d]	980	+0.50	+6.60	0.82	95, 168, 8
		Calculated: Nonrelativistic (Ideal D_{4d} $Mo(CN)_8^{4-}$ anion)			
−1263	722	+1.00	+6.92	0.00	90, 0, NA[e]

[a] Calculated isotropic chemical shifts were determined using $\delta(\text{ref})_{iso,calc} = -1860.0$ ppm for $Mo(CO)_6$ and $\delta(\text{sample})_{iso,calc} = \sigma(\text{ref})_{iso,calc} - \sigma(\text{sample})_{iso,calc} - 1860.0$ ppm [b] ZORA DFT calculations using QZ4P basis sets were performed on the isolated $Mo(CN)_8^{4-}$ anion using coordinates as determined from X−ray crystallography. [c] Spin−orbit: for $Mo(CO)_6$, $\sigma(\text{ref})_{iso,calc} = 1572.3$ ppm and $\delta(\text{ref})_{iso,calc} = -1860$ ppm. [d] Nonrelativistic: for $Mo(CO)_6$, $\sigma(\text{ref})_{iso,calc} = 1229.4$ ppm and $\delta(\text{ref})_{iso,calc} = -1860$ ppm. [e] Due to the axial symmetry of the CS and EFG tensors, the calculated line shape for the ^{95}Mo NMR spectrum is invariant to angle, γ.

an ideal square antiprism; instead, the ^{95}Mo NMR spectrum for $Tl_4Mo(CN)_8$ is more than twice the breadth of that for $K_4Mo(CN)_8 \cdot 2H_2O$.

According to the crystal structure for $Tl_4Mo(CN)_8$,[17] structural deviations present in the anion are significant, reducing the point group symmetry from D_{4d} to C_1. The average parameters determined from the X-ray diffraction study[17] are: $r(Mo,C)_{avg} = 2.150 \pm 0.019$ Å, $r(C,N)_{avg} = 1.163 \pm 0.013$ Å, and $(\angle Mo,C,N)_{avg} = 175.8 \pm 1.8°$. The parameter which deviates most from ideal symmetry is the Mo−C−N bond angle, which must be 180° for a square antiprismatic structure. Deviations from square antiprismatic symmetry are evident in the ^{13}C (not shown; MAS sample) NMR spectra of $Tl_4Mo(CN)_8$; at 11.75 T, the eight carbon atoms are not fully resolved, resulting in overlapping ^{13}C NMR signals with chemical shifts varying over approximately 15 ppm between 147 and 162 ppm; however, if the structure were truly a square antiprism, a single carbon peak would appear in the ^{13}C NMR spectrum. These structural deviations were, therefore, initially thought to explain the large, observed EFG at Mo for $Tl_4Mo(CN)_8$.

Similar to the K salt, nonrelativistic and spin−orbit relativistic ZORA DFT calculations were carried out on the isolated $Mo(CN)_8^{4-}$ anion using the structure determined from a single-crystal X-ray diffraction study,[17] i.e., approximate D_{4d} symmetry, and are summarized in Table 2. The calculated results are in good agreement with experiment and also predict a significant EFG at Mo and a large Mo shielding anisotropy. The main discrepancy between the best-fit and calculated parameters are the values for η_Q; nevertheless, the calculations are correct in predicting a large deviation from axial symmetry. Inclusion of the first coordination sphere of four Tl cations (within a distance of 4.85 Å from Mo) in the nonrelativistic ZORA DFT calculation does not significantly alter the EFG and σ parameters: $C_Q = 6.21$ MHz, $\eta_Q = 0.70$, $\sigma_{iso} = 801.4$ ppm, $\Omega = 741$ ppm, and $\kappa = +0.65$.

While deviations from square antiprismatic symmetry for $Tl_4Mo(CN)_8$ are significant, the magnitude of the Mo EFG is larger than anticipated. The individual contributions from the Mo σ and EFG interactions to the ^{95}Mo NMR spectra, obtained from the best-fit experimental parameters in Table 2, are illustrated in Figure 6. The observed EFG at Mo for $Tl_4Mo(CN)_8$ is $C_Q = (+)6.35$ MHz; again, the sign of $C_Q(^{95}Mo)$ was inferred from the DFT calculations. The span of the Mo shielding tensor for the Tl salt, 1350 ppm, represents the largest reported value for Mo. For $Tl_4Mo(CN)_8$, the crystal

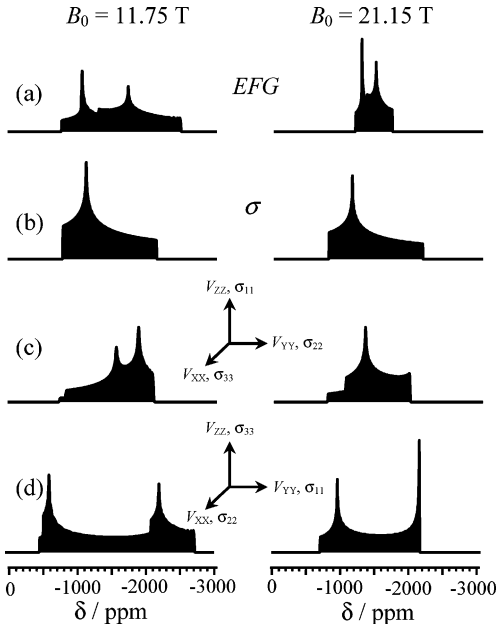

Figure 6. Simulations of central transition ^{95}Mo NMR spectra of solid, stationary $Tl_4Mo(CN)_8$ to show the contributions from the EFG (a) and σ (b) interactions. The sum of these interactions is shown (c, d) using two possible relative orientations of the EFG and σ tensors. Simulations which best match the experimental spectra are shown in (d). Simulation parameters are given in Table 2.

symmetry does not dictate the relative orientations of the σ and EFG tensors; hence, the Euler angles were obtained by manual iteration and visual comparison with the experimental ^{95}Mo NMR spectra obtained at 11.75 and 21.15 T. Two arbitrary orientations are shown in Figure 6, c and d, to illustrate the sensitivity of the line shape on the Euler angles. The simulation which best fits the experimental spectra corresponds to the relative orientation of EFG and σ tensors where: $V_{XX} \parallel \sigma_{22}$, $V_{YY} \parallel \sigma_{11}$, and $V_{ZZ} \parallel \sigma_{33}$, shown in Figure 6d. That the principal components of the EFG and σ tensors are, within experimental error, coincident is fortuitous since the crystal symmetry does not dictate such an orientation for $Tl_4Mo(CN)_8$; however, the excellent fits obtained at 11.75 and 21.15 T support this solution. According to the ZORA DFT calculations for the anion in $Tl_4Mo(CN)_8$ (Table 2), the σ and EFG tensors have the same general orientation as that determined by experiment, with slight deviations from coincidence (<10°) between principal components of the σ and EFG tensors.

The values obtained for the Mo EFG and the span of the Mo shielding tensor for $Tl_4Mo(CN)_8$ are surprisingly comparable to those observed for $K_4Mo(CN)_8 \cdot 2H_2O$. In previous ^{95}Mo NMR studies of $K_4Mo(CN)_8 \cdot 2H_2O$ dissolved in isotropic liquids, results were interpreted on the strict basis that the D_{4d} structure has a zero EFG; however, our solid-state ^{95}Mo NMR results indicate that, when structural deviations are considered, not only is the EFG at Mo non-zero, it is significant and comparable in magnitude to that observed for the D_{2d} structure.

Although the magnitudes of the σ and EFG parameters are similar for $K_4Mo(CN)_8 \cdot 2H_2O$ and $Tl_4Mo(CN)_8$ (Tables 1 and 2), the symmetry and sign of these tensors differ considerably. The sign of C_Q is negative for D_{2d} $K_4Mo(CN)_8 \cdot 2H_2O$, but positive for D_{4d} $Tl_4Mo(CN)_8$, and the skew of the magnetic shielding tensor is also different. The σ tensor for $K_4Mo(CN)_8 \cdot 2H_2O$ is near axial symmetry, with σ_{11} being the unique component ($\kappa = -0.987$), while the skew is reversed for $Tl_4Mo(CN)_8$. For the Tl salt, the σ tensor deviates considerably from axial symmetry, with a positive skew, $\kappa = +0.5$, and principal components, $\delta_{11} = -788$ ppm, $\delta_{22} = -1125$ ppm, and $\delta_{33} = -2138$ ppm. The relative orientation of the Mo σ and EFG tensors for the two salts is also different. In each case, the principal components of the σ and EFG tensors are coincident, and V_{ZZ} must be parallel to the highest molecular symmetry axis; however, the exact orientation of the tensors is different for the two salts (see Figures 3d and 6d).

It is interesting to compare the Mo shielding tensors for the D_{2d} and D_{4d} Mo(CN)$_8^{4-}$ to the g tensors for the analogous paramagnetic Mo(V) systems. While NMR spectroscopy has been used to investigate the structure of diamagnetic Mo(CN)$_8^{4-}$ anions, ESR has similarly been used to study the structure of Mo(CN)$_8^{3-}$ anions.[15,96,94,100,101] In one ESR investigation,[96] the authors calculated the ordering of d orbitals for ideal D_{2d} and D_{4d} symmetry to determine the sense of the g tensors to rationalize the structure of Mo(CN)$_8^{3-}$. They concluded that d(x^2-y^2) is the ground−state orbital for D_{2d} symmetry, while d(z^2) is the ground-state orbital for D_{4d} symmetry, in agreement with our ZORA DFT calculations for the ideal D_{2d} and D_{4d} Mo(CN)$_8^{4-}$ anions (Figure 1). They further determined that the anisotropic g tensors are axially symmetric with $g_\perp > g_\parallel$ for D_{2d} symmetry and $g_\parallel > g_\perp$ for D_{4d} symmetry. Hence, just as the sense of the σ tensor changes for the diamagnetic D_{2d} and D_{4d} Mo(CN)$_8^{4-}$ anions, the sense of the g tensors changes for the analogous paramagnetic systems.

Initially, the lowered symmetry in $Tl_4Mo(CN)_8$ was presumed to explain the non-zero EFG at Mo ($C_Q = +6.35$ MHz) and the disagreement with the PCA. To investigate this further, EFG and σ tensor calculations were carried out on idealized models of Mo(CN)$_8^{4-}$ with D_{4d} symmetry (Table 2). Surprisingly, the calculated results for square antiprismatic Mo(CN)$_8^{4-}$ indicate that the large EFG at Mo remains, but the Mo EFG tensor is now axially symmetric, as expected. Before discussing the non-zero EFG further, the calculated magnetic shielding anisotropy for the Mo(CN)$_8^{4-}$ anion possessing square antiprismatic symmetry will be discussed.

Similar to the strategy used for the K salt, the large anisotropy in the Mo shielding tensor for $Tl_4Mo(CN)_8$ is rationalized in terms of the paramagnetic shielding contributions to the principal components of the magnetic shielding tensor; the following results pertain to the ideal square antiprismatic Mo(CN)$_8^{4-}$ anion. The reader is referred to selected energy levels for square antiprismatic Mo(CN)$_8^{4-}$, shown in Figure 1b. Recalling that the Mo shielding tensor for $Tl_4Mo(CN)_8^{4-}$ is oriented such that σ_{33} is along the z-axis and σ_{22}, σ_{11} are along the x,y-axes, respectively, indicates that contributions to σ_{22}, σ_{11} involve rotations about the x,y-axes, thereby mixing d(z^2) with d(xz) and d(yz) (Figure 7). This mixing involves the two lowest energy gaps, is both allowed[98] and favorable, and is responsible for the deshielding of σ_{11} and σ_{22}. Contributions to σ_{33} involve mixing of the d(xy) and d(x^2-y^2) orbitals via $\hat{L}_z$. The smaller paramagnetic contribution to σ_{33} results from the larger energy gaps between occupied (HOMO−3,−4) and virtual (LUMO,+1,+7,+8) orbitals of Mo d(xy) and d(x^2-y^2) character.

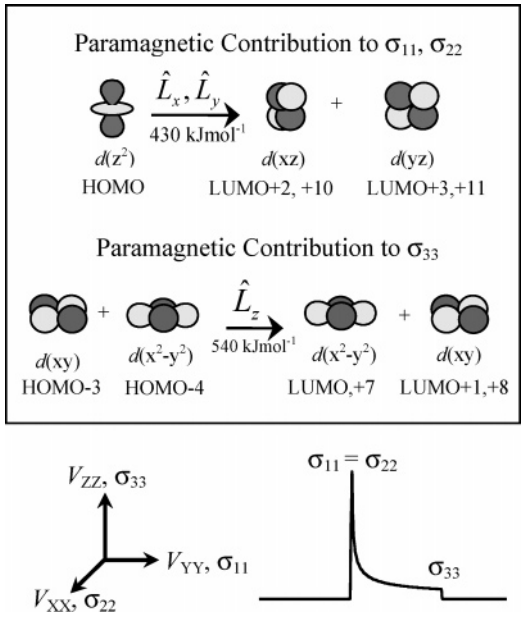

Figure 7. Origin of the paramagnetic shielding contribution to the principal components of the Mo magnetic shielding tensor, σ_{ii}^{para}, for D_{4d} Mo(CN)$_8^{4-}$. Symmetry-allowed mixing between occupied and virtual Mo d-dominated molecular orbitals via the angular momentum operators, $\hat{L}_x$, $\hat{L}_y$, and $\hat{L}_z$ give rise to σ_{ii}^{para}. The relative orientation of the Mo σ and EFG tensors in the molecular frame (i.e., V_{XX}, V_{YY}, and V_{ZZ} are coincident with the x-, y-, z-axes), along with the Mo σ powder pattern, are shown to help visualize and rationalize the mixing of d orbitals.

Contributions from the total diamagnetic and paramagnetic terms result in an overall deshielding for square antiprismatic Mo(CN)$_8^{4-}$, $\sigma_{iso} = 1020$ ppm (spin−orbit relativistic; Table 2), with respect to the bare Mo nucleus, $\sigma_{iso} \approx 4317.7$ ppm.

4.3 Quantum Chemical Investigation of the D_{4d} Mo(CN)$_8^{4-}$ Anion: Investigation of the PCA. To test the reliability of the DFT calculations of the Mo EFG and σ tensors for Mo(CN)$_8^{4-}$, which indicate a significant EFG at Mo for both approximate and ideal square antiprismatic symmetry and are in disagreement with the PCA, calculations of Mo EFG and σ tensors were performed on representative Mo compounds of ideal symmetry, namely, the tetrahedral molybdate anion in Na_2MoO_4,[84] the tetrathiomolybdate anion in $[(C_2H_5)_4N]_2[MoS_4]$,[85] the tetraselenomolybdate anion in $[(C_6H_5)_4P]_2[MoSe_4]$,[86] and the octahedral molecule, $Mo(CO)_6$.[87] The experimental Mo chemical shift values of these compounds cover approximately 60% of the chemical shift range for molybdenum. Our calculations were performed on isolated, idealized structures of these

(100) Hayes, R. G. *J. Chem. Phys.* **1966**, *44*, 2210−2212.
(101) McGarvey, B. R. *Inorg. Chem.* **1966**, *5*, 476−479.

Table 3. Calculated NMR Parameters for Isolated, Idealized Model Compounds of High Symmetry and Experimental Mo Chemical Shift Values

symmetry	molecule	$\delta_{iso,exp}$/ ppm	$\delta_{iso,calc}$/ ppm[a,b]	σ_{iso}/ ppm	C_Q/MHz	η_Q
T_d	MoO_4^{2-}	0	347	−636	0.00	−
T_d	MoS_4^{2-}	2259[102]	2282	−2571	0.00	−
T_d	$MoSe_4^{2-}$	3145[102]	2970	−3259	0.00	−
O_h	$Mo(CO)_6$	−1860	−1860	1571	0.00	−
O_h	$Mo(CN)_8^{4-}$	−	−1287[c]	656	0.00	−
D_{4d}	$Mo(CN)_8^{4-}$	−1375	−1263	974	+6.92	0.00
D_{2d}	$Mo(CN)_8^{4-}$	−1350	−1212	923	−7.47	0.00

[a] ZORA DFT spin−orbit calculations using QZ4P basis sets. [b] Calculated isotropic chemical shifts were determined using $\delta(\text{ref})_{iso,calc} = -1860.0$ ppm for $Mo(CO)_6$ and $\delta(\text{sample})_{iso,calc} = \sigma(\text{ref})_{iso,calc} - \sigma(\text{sample})_{iso,calc} - 1860.0$ ppm. [c] The spin−orbit relativistic calculation for O_h $Mo(CN)_8^{4-}$ did not converge; hence, nonrelativistic ZORA DFT was employed using QZ4P basis sets. An analogous calculation was carried out on the secondary reference, $Mo(CO)_6$: $\sigma_{iso} = 1229.4$ ppm, $\delta_{iso} = -1860$ ppm, to determine the calculated chemical shift for O_h $Mo(CN)_8^{4-}$ QZ4P basis sets were used.

Mo compounds, as well as $Mo(CN)_8^{4-}$ anions possessing D_{2d}, D_{4d}, and O_h symmetry; the results are summarized in Table 3. Considering that the calculations were performed on isolated molecules or anions with ideal symmetry and do not account for solvent effects, our calculated δ_{iso} values are in good agreement with experimental values.[67,102] Furthermore, results for the calculated Mo EFG tensor for compounds of T_d and O_h symmetry are in accord with the PCA in that a zero EFG is predicted; however, a significant EFG is calculated for the isolated $Mo(CN)_8^{4-}$ anion possessing square antiprismatic (D_{4d}) symmetry, contrary to the PCA which indicates the EFG at Mo is necessarily zero.

Initially, the origin of the non-zero EFG at Mo for the isolated square antiprismatic $Mo(CN)_8^{4-}$ anion was thought to arise from the two d electrons localized in Mo d(z^2) atomic orbitals. To investigate this further, calculations were performed on isolated $Mo(CN)_8^{2-}$, where the formal charge on Mo is +6 and there are no valence d electrons; however, nonrelativistic calculations indicate that the large EFG in the Mo(VI) system remains and is slightly larger ($C_Q = -8.4$ MHz) than that for the Mo(IV) anion. In the hypothetical Mo(VI) system, the highest occupied MOs have zero contribution from Mo 4d orbitals,whereas the lowest unoccupied MOs are largely dominated by Mo d orbitals. Hence, it appears that the valence d electrons are not the source of the EFG for either the Mo(IV) or the Mo(VI) system. Similar results were found when calculations were performed on $Zr(CN)_8^{4-}$, a hypothetical anion where Zr is ideally d^0. In this case, both the standard ZORA DZ basis set for Zr and a modified Zr basis set, in which all 4d orbitals were removed, were employed. In both cases, the calculations yield an EFG at Zr that is large but is several times smaller than the analogous Mo calculation using standard ZORA DZ basis sets: $eq_{ZZ}(^{91}Zr)_{DZ} = 0.37 \times 10^{21}$ V m^{-2}, $eq_{ZZ}(^{91}Zr)_{\text{modified DZ}} = 0.15 \times 10^{21}$ V m^{-2}, and $eq_{ZZ}(^{95}Mo)_{DZ} = 0.79 \times 10^{21}$ V m^{-2}. These results indicate that the large EFG is not solely linked to the d electrons. Last, a ZORA DFT EFG calculation was carried out on MoF_8^{4-}, and again, a large EFG was computed, indicating that the extended CN^- ligand is not the source of the EFG at Mo.

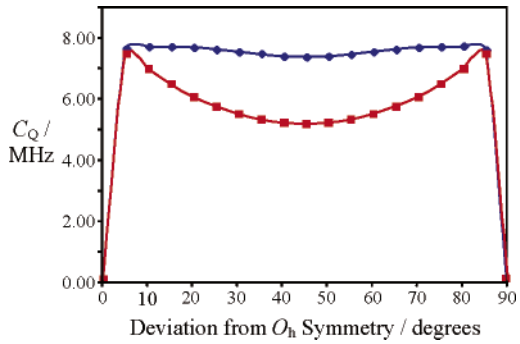

Figure 8. Nonrelativistic $C_Q(^{95}Mo)$ values for $Mo(CN)_8^{4-}$ rotamers as a function of deviation from cubic symmetry. Using the PCA, a zero EFG at Mo results for all rotamers. ZORA DFT calculations, ◆ (blue), and RHF, ■ (red), calculations.

Failure of the PCA for the above cases motivated us to carry out a calculation using actual point charges, q_i, in lieu of the CN^- ligands. This involved replacing each carbon and nitrogen atom with a point charge, equivalent to the charge predicted by RHF calculations, such that the overall molecular charge for the "anion", $Mo(q_C q_N)_8^{4-}$ is −4. The calculated result is in accord with the PCA with a zero EFG for D_{4d} symmetry. This implies that the asymmetry in the distribution of the ligand charge gives rise to the non-zero EFG at Mo and Zr.

Since the PCA holds for cubic $Mo(CN)_8$,$^{4-}$ but fails for the square antiprismatic analogue, we carried out calculations of the Mo EFG tensor during the transition from O_h to D_{4d} symmetry in an attempt to understand the EFG at Mo for D_{4d} $Mo(CN)_8$.$^{4-}$ Both nonrelativistic ZORA DFT and RHF calculations of the Mo EFG tensor for various rotamers of $Mo(CN)_8^{4-}$ were carried out. The $Mo(CN)_8^{4-}$ anion possessing cubic symmetry served as our starting structure, and subsequent rotamers were generated by rotating the top portion of the cube in steps of 5° about the principal, z-axis, while holding the bottom fragment of the cube fixed. A total of 10 rotamers were generated from O_h $Mo(CN)_8^{4-}$, each possessing D_{4d} symmetry, with the square antriprism (Figure 1b) representing our final structure. Shown in Figure 8 is a plot of the calculated $C_Q(^{95}Mo)$ values as a function of deviation from cubic symmetry. According to the PCA, the EFG at Mo is zero for *all* rotamers, including the square antiprism; however, the DFT and RHF calculations indicate that once the cubic symmetry of $Mo(CN)_8^{4-}$ is broken, a dramatic increase in the EFG is observed. The EFG at Mo remains high but slowly decreases and reaches a local minimum at 45°, i.e., the square antiprism. The general agreement in the trends for the calculated EFGs at Mo obtained using two methods is reassuring. In particular, both methods calculate axially-symmetric Mo EFG tensors for all rotamers and a zero EFG at Mo for O_h symmetry, but a non-zero and substantial EFG at Mo for square antiprismatic symmetry, lending confidence to our calculated and experimental results. Nevertheless, according to the PCA, *both* O_h and square antiprismatic symmetries should result in a zero EFG.[65]

Magnetic shielding calculations were also carried out on the above D_{4d} $Mo(CN)_8^{4-}$ rotamers (Figure 9). Results for O_h $Mo(CN)_8^{4-}$ are not shown in Figure 9 since this calculation required use of a higher basis set for convergence. The principal components of the Mo σ tensor are shown in Figure 9, where it is clear that σ_{33} largely governs both the isotropic and anisotropic magnetic shielding. The profiles of σ_{iso} and Ω for

(102) Brevard, C.; Pregosin, P. S.; Thouvenot, R. In *Transition Metal Nuclear Magnetic Resonance*; Pregosink, P. S., Ed.; Elsevier: Amsterdam, 1991; pp 67−81.

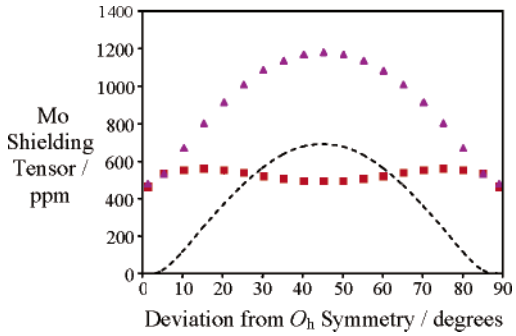

Figure 9. Components of the axially symmetric Mo shielding tensor, $\sigma_{11} = \sigma_{22}$ ■ (red), σ_{33} = ▲ (purple), and span = -- - -, for Mo(CN)$_8^{4-}$ rotamers as a function of deviation from ideal cubic symmetry, calculated using nonrelativistic ZORA DFT.

the rotamers show a steady increase upon rotation from O_h symmetry, with maxima at square antiprismatic symmetry. The increase in the anisotropic shielding can be understood by considering the orientation of the shielding tensors and inspecting the contribution from the paramagnetic shielding, σ_{para}, to the principal components for each rotamer. In each case, σ_{33} is collinear with the *z*-axis; hence, contributions from σ_{para} to σ_{33} involve mixing of d(xy) and d(x^2-y^2) orbitals via $\hat{L}_z$, whereas mixing of d(z^2) and d(xz), d(yz) via $\hat{L}_x$ and $\hat{L}_y$ contribute to σ_{11}, σ_{22}. The increase in σ_{33} upon increased deviation from O_h symmetry is due to an increase in the energy gap involving d(xy) and d(x^2-y^2) orbitals, as well as a gradual decrease in the percent contribution of these atomic orbitals to the molecular orbitals; the end result is a decrease in the contribution of σ_{para} to σ_{33} and, thus, an increase in σ_{33}. The paramagnetic contribution to σ_{11} and σ_{22} remains relatively constant upon rotation as the molecular orbitals involving Mo d(z^2), d(xz), and d(yz) atomic orbitals do not change significantly during the transition from O_h to square antiprismatic symmetry for the Mo(CN)$_8^{4-}$ rotamers.

5. Conclusions

Solid-state ^{95}Mo NMR spectroscopy is an ideal method for examining the two forms of Mo(CN)$_8^{4-}$ anions possessing approximate dodecahedral and square antiprismatic symmetry. The magnitudes of the Mo EFG and magnetic shielding anisotropy are significant for both $K_4Mo(CN)_8 \cdot 2H_2O$ and $Tl_4Mo(CN)_8$; however, the sign and relative orientations of the EFG and magnetic shielding tensors result in ^{95}Mo NMR spectra which are strikingly different for the two forms. Our calculations on Mo(CN)$_8^{4-}$ anions possessing ideal dodecahedral and square antiprismatic symmetry indicate a substantial EFG at Mo for *both* structures; this result is in contrast to the PCA, which predicts a zero EFG for D_{4d} Mo(CN)$_8^{4-}$ and a non-zero EFG for D_{2d} Mo(CN)$_8^{4-}$. Although the origin of the non-zero EFG for square antiprismatic Mo(CN)$_8^{4-}$ is not clear, our calculations indicate it does not exclusively arise from the Mo d electrons or the diatomic nature of the cyanide ligand. High-level quantum chemical calculations have provided insight into the origin of the large EFG and Mo magnetic shielding anisotropies in $K_4Mo(CN)_8 \cdot 2H_2O$ and $Tl_4Mo(CN)_8$ and allowed the Mo magnetic shielding and EFG tensors, as well as their relative orientations, to be characterized.

Acknowledgment. The ^{95}Mo NMR spectra acquired at 17.63 and 21.1 T were obtained at the Environmental Molecular Sciences Laboratory (EMSL) located at Pacific Northwest National Laboratory, operated by Battelle for the D.O.E. The QCPMG/DFS ^{95}Mo NMR spectrum of $Tl_4Mo(CN)_8$ acquired at 21.1 T was collected by Dr. Andrew S. Lipton. We are grateful to the staff at EMSL: Andy Lipton, Jesse Sears, Nancy Isern, David Hoyt, Joe Ford, and Paul Ellis, for their help and hospitality. We also thank the members of the solid-state NMR group at the University of Alberta and Dr. Klaus Eichele for interesting discussions on this research, with a special thanks to Dr. Devin Sears for the RHF calculations. Profs. Alex Brown (University of Alberta) and Jochen Autschbach (University of Buffalo) are thanked for their assistance with some EFG calculations, and Mathew J. Willans and Richard Warren are thanked for their efforts in synthesizing $K_4Mo(CN)_8 \cdot 2H_2O$. R.E.W. is a Canada Research Chair in physical chemistry. We thank the Natural Sciences and Engineering Research Council of Canada, the Alberta Ingenuity Fund, and the University of Alberta for financial support.

Supporting Information Available: Cartesian coordinates and expansion of Figure 2. This material is available free of charge via the Internet at http://pubs.acs.org.

JA060124X